Catalytic Oxidation of NO by Ozone over Mn-Ce/Al$_2$O$_3$/TiO$_2$ Catalyst

Hong Shen [1], Zijun Tang [2], Xiang Xiao [2], Haiwen Wu [2], Hang Zhou [3], Ping Fang [2], Dingfang Zhu [4] and Jianhua Ge [1],*

[1] School of Earth and Environment, Anhui University of Science and Technology, Huainan 232001, China
[2] South China Institute of Environmental Sciences, Ministry of Ecology and Environment, Guangzhou 510655, China
[3] Guangzhou Likun Environmental Protection Technology Development Co., Ltd., Guangzhou 510700, China
[4] Nanjing Lishui District Environmental Monitoring Station, Nanjing 210000, China
* Correspondence: gejianhua13@163.com; Tel.: +86-18715699964

Abstract: In this study, Mn-Ce/Al$_2$O$_3$/TiO$_2$ catalyst prepared by impregnation method was used for synergistic O$_3$ oxidation NO. The catalyst prepared by impregnating Al$_2$O$_3$/TiO$_2$ at a Mn:Ce molar ratio of 4:1 showed the best catalytic activity. The catalyst performance showed that when the molar ratio of Mn:Ce was 4:1 and the volume ratio of O$_3$:NO was 1:4, the removal rate of NO could reach 63%, which could increase the removal rate by 40% compared with that of NO oxidized by O$_3$ alone. BET, XRD, and TEM characterization results showed that when the molar ratio of Mn:Ce was 4:1, the catalyst specific surface area, and pore capacity were the largest. A large amount of MnOx and CeOx were distributed on the catalyst surface. The XPS analysis showed that the oxidation-reduction and oxygen vacancy of Mn (IV)/Mn (III)/Mn (II) and Ce (IV)/Ce (III), had a synergistic effect on the decomposition of O$_3$ into reactive oxygen species(O*), thus improving the catalytic capacity of Mn-Ce/Al$_2$O$_3$/TiO$_2$ catalyst for O$_3$. The O$_2$-TPD analysis showed that the oxygen vacancies and oxygen species in the catalyst could be used as the active point of decomposition of O$_3$ into O*. The experimental results show that the prepared catalyst can significantly improve the efficiency of ozone oxidation of NO and reduce the amount of ozone. The catalyst can be applied to ozone oxidation denitrification technology.

Keywords: Mn-Ce-based catalyst; catalytic oxidation of NO; process analysis

1. Introduction

With the development of society, the energy demand is increasing. Clean energy, renewable energy, etc., are constantly proposed, and traditional energy sources are mainly non-renewable resources such as coal and oil. Biomass is a new environmentally friendly fuel that is gradually being used. Biomass energy has the advantages of easy storage, stable combustion, and low pollutant emissions compared to traditional energy sources [1,2]. Nowadays, the use of biomass energy is increasing [3–5], such as oil palm, coconut shells, grains, livestock manure, green waste, etc. [6,7]. At present, the main application scenario of biomass in China is mainly boiler combustion, and the mixture of biomass and traditional coal combustion can reduce NO and SO$_2$ emissions [8,9]. Although the concentration of air pollutants emitted from biomass boilers is lower compared to traditional coal-fired boilers, existing studies show that NOx emissions from biomass boilers are between 200–500 mg/m^3, and meeting the emission standards still requires treatment. At present, most biomass boilers in China have not carried out flue gas denitrification. A small number of enterprises use traditional SNCR denitrification technology, but there are a series of problems such as corrosion of the boiler. A small number of enterprises use SCR denitrification technology, but there are problems such as easy clogging and catalyst poisoning [10]. Some enterprises also use ozone (O$_3$) oxidation denitrification technology, but there are problems such as high O$_3$ consumption and high operating costs. At present,

China lacks economical and efficient treatment technologies for the removal of flue gas nitrogen oxides from biomass boilers.

Given this aforementioned problem, relevant researches have been carried out at home and abroad. One of the directions is to develop suitable catalysts to improve the oxidation performance of O_3 and reduce the usage of O_3. O_3 oxidation for the removal of pollutants generally works in conjunction with associated catalysts to achieve high removal efficiencies. O_3 oxidation efficiency is mainly affected by O_3 concentration and flue gas temperature [11]. For common active components of catalysts, such as Mn-based catalysts, Mn mainly contributes to the decomposition of O_3 into reactive oxygen ions to participate in oxidation [12]. Low oxidation state Mn compounds in Mn/γ-Al_2O_3 catalyst contribute to the decomposition of O_3 to promote the oxidation of pollutants [13]. Under the co-treatment of NO by TiO_2 catalyst and a high concentration of O_3, the TiO_2 catalyst contributes to the transformation of NO_2 into N_2O_5 [14]. When the volume ratio of O_3:NOx > 1.57, the oxidation rate of NO can reach 95% under the synergistic action of $MnOx/Al_2O_3$ catalyst and O_3 [15], but too high a concentration of O_3 can produce leaks. V_2O_5-$(NH_4)_2V_6O$ [16] catalyst was used to synergistically oxidize NO with O_3, when the volume ratio of NO: O_3 = 2:1, the oxidation efficiency of NO could be the highest, and the O_3 escape was less than 1 ppm 16. In terms of flue gas treatment, after flue gas was treated by wet flue gas desulfurization (WFGD), Mn-Ce/TiO_2 catalyst was used to oxidize NOx with O_3, and the removal rate of NOx could reach 77.1% [17]. The synergy of O_3 and catalyst has a good effect on the treatment of gas pollutants. In practical application, it is risky to use a high concentration of O_3 in pollutant treatment, and it costs a lot to the economy. Therefore, it is necessary to prepare catalysts that can adapt to lower O_3 concentrations and have higher treatment efficiency.

The purpose of this experiment is to study the effect and process mechanism of catalysts promoting O_3 oxidation of NO. Catalysts with different ratios of active components (Mn:Ce = 1:2, Mn:Ce = 2:1, Mn:Ce = 4:1, Mn:Ce = 5:1) were prepared by impregnation method. The performance of catalysts was investigated by different characterization methods, and the mechanism of catalysts to enhance ozone oxidation of NO was researched. The study can provide theoretical data support for the research on ozone oxidation denitrification technology of biomass boiler flue gas.

2. Materials and Methods

2.1. Preparation of Catalysts

Mn-Ce was selected as the main active component of the catalyst and prepared by the impregnation method. $Mn(NO_3)_2$ and $CeN_3O_9 \cdot 6H_2O$ were used as reagents, and nano titanium dioxide and Al_2O_3 were used as carriers. The carrier molar ratio was m (Al_2O_3):m (TiO_2) = 1:1, the mess ratios of m (active component):m (carrier) = 1:1. The active component molar ratios were n (Mn:Ce) = 1:2, n (Mn:Ce) = 2:1, n (Mn:Ce) = 4:1, n (Mn:Ce) = 5:1, and the relevant information of the reagents are shown in Table 1. The weighed $Mn(NO_3)_2$ and $CeN_3O_9 \cdot 6H_2O$ were fully mixed in 40 mL deionized water, and then the carrier was added, fully mixed, and stirred for 4 h at 700 RPM. After mixing, the water was filtered and washed alternately with C_2H_6O and deionized water. Then, it was placed in a 100 °C oven and dried for 2 h, then calcined for 2 h in a muffle oven at 300 °C, cooled, removed, and finally ground and screened. Mn-$Ce/Al_2O_3/TiO_2$ catalysts with different proportions of active components were prepared (Mn:Ce = 1:2, Mn:Ce = 2:1, Mn:Ce = 4:1, Mn:Ce = 5:1 referred to as catalysts).

Table 1. Reagents used in the experiments and purity.

Name of the Reagent	Source of Reagent	Purity
$Mn(NO_3)_2$	Maclean Biochemical Technology Co., Ltd., Shanghai, China	AR
$CeN_3O_9 \cdot 6H_2O$	Aladdin Biochemical Technology Co., Ltd., Shanghai, China	99.95%
Nano titanium dioxide	Hechan Trading Co., Ltd., Guangzhou, China	AR
Al_2O_3 (α-crystalline about 90%, γ-crystalline about 10%)	Damao Chemical Reagent Factory., Tianjing, China	AR
C_2H_6O	Lingfeng Chemical Reagent Co., Ltd., Shanghai, China	AR

2.2. Experimental Setup

The experimental setup consists of O_3 generator and catalytic oxidation adsorption platform, as shown in Figure 1.
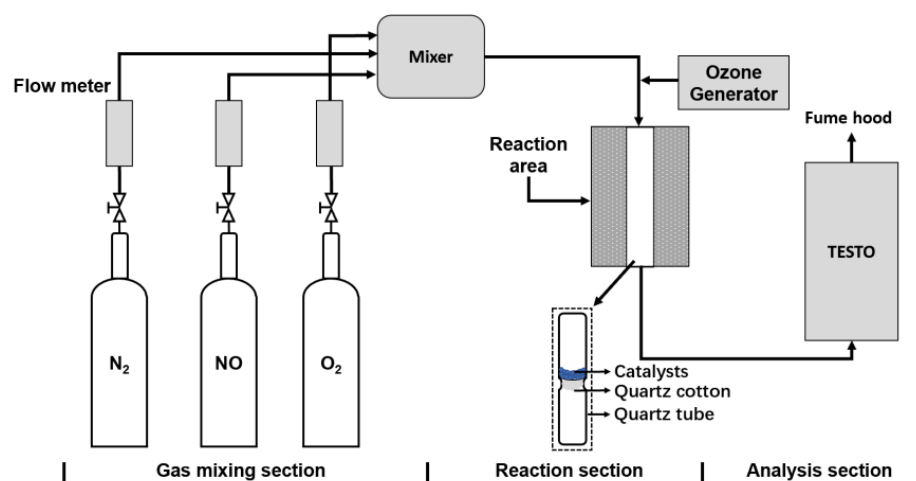
Figure 1. Experimental setup and flow chart.

The O_3 required for the experiment was generated from an ozone generator (Feige Environmental Protection Technology Co., Ltd., Guangzhou, China). After the concentration of O_3 was measured by the ozone analyzer (Zhipu Automation Technology Co., Ltd., Zibo, China), it was passed into the catalytic oxidation adsorption platform. The gas pipeline in the experimental platform was mainly stainless steel, and the gas inflow rate was controlled by a flow meter. N_2 (99.9% N_2, Yuejia Gas Co., Ltd., Guangzhou, China), NO (4.01% NO + nitrogen balance, Yuejia Gas Co., Ltd., Guangzhou, China), and O_2 (99.9% O_2, Yuejia Gas Co., Ltd., Guangzhou, China) were mixed in the mixing zone. The mixer can be heated and kept warm as needed. The simulated flue gas was mixed with O_3 before entering the reactor. A quartz tube was placed in the middle of the reactor, and quartz wool was arranged in the middle of the quartz tube as support. The catalyst was evenly placed on the upper part of the quartz wool. During the experiment, the gas passed through the catalyst from top to bottom, and after the gas reacted, the change in the concentration of the exhaust gas was detected by the TESTO 350.

2.3. Catalyst Performance Test

The simulated total flue gas flow rate was 1 L/h, O_2 concentration was 13%, and the volume ratio of O_3:NO = 1:2, 1:3, 1:4, the O_3 flow rate was 1 L/h, a total of 2 L gas passes through the catalyst, and gas hourly space velocity (GHSV) was 60,000 h^{-1}. The initial

incoming NO concentration was 300 ppm, and the O_3 concentration was 100 ppm. By adjusting different O_3:NO ratios, the main oxidation efficiency was expressed as $NO_{[removal]}$.

$$NO_{[removal]} = \frac{NO_{[a]} - NO_{[b]}}{NO_{[a]}} \times 100\%, \tag{1}$$

where $NO_{[a]}$ was the concentration of NO at the inlet; $NO_{[b]}$ was the concentration at the exit of O_3 (with catalyst).

The main mechanism of the reaction between O_3 and NO was as follows [14]:

$$NO + O_3 \rightarrow NO_2 + O_2, \tag{2}$$

$$NO_2 + O_3 \rightarrow NO_3 + O_2, \tag{3}$$

$$NO_2 + NO_3 \rightarrow N_2O_5, \tag{4}$$

$$N_2O_5 \rightarrow NO_3 + O_2, \tag{5}$$

$$NO + NO_3 \rightarrow 2NO_2, \tag{6}$$

2.4. Characterization of Catalysts

Specific surface area and pore size were determined by Micromeritics ASAP 2020 Surface Area and Porosity Analyzer. XRD using D8 ADVANCE X-ray diffractometer from Bruker, Germany. TEM was measured using a JEM 2100F instrument with an accelerating voltage of 200 KV and an electron wavelength of 0.0251 Å. XPS was determined using Thermo Scientific Escalab 250Xi. O_2-TPD was determined using MicroActive for AutoChem II 2920 Version 6.01.

3. Results

3.1. Morphology Analysis of Catalysts

Table 2 mainly shows the BET surface area, total pore volume, and average pore size of Mn-Ce/Al_2O_3/TiO_2 catalyst samples with different active component ratios. The specific surface area and pore volume of the catalyst reached the maximum when the molar ratio of Mn:Ce =4:1, but when Mn:Ce =5:1, the specific surface area and pore size of the catalyst began to decrease. The results indicated that when the molar ratio of Mn:Ce =4:1, the carrier has reached the maximum load, and the active component cannot be fully loaded on the carrier when Mn is excessive, and the loading effect is poor. Figure 2a,b shows the N_2 adsorption-desorption isotherms and corresponding pore size distribution curves of Mn-Ce/Al_2O_3/TiO_2. It can be seen from Figure 2a that the N_2 adsorption and desorption isotherms of Mn-Ce/Al_2O_3/TiO_2 with different ratios of active components showed similarly. The first half of the isotherm was similar to the type II isotherm, and the second half was the type IV (a) isotherm, which was the combination of type II and type IV (a), which indicated that there were mesopores (2~50 nm) in the sample. In the relative pressure (P/P_0) range of 0.8~1.0, the shape of the hysteresis loop on the IV (a) isotherm was H3 type. The H3-type hysteresis loop was formed by the stacking of nanoblocks, which indicated the presence of fracture holes, and this analysis was consistent with the results of the TEM (Figure 3). In addition, Mn-Ce/Al_2O_3/TiO_2 has higher adsorption at the relative pressure (P/P_0) of 1, indicated that the sample contains macropores. Figure 2b shows the pore size distribution of the sample. It can be seen from the figure that Mn-Ce/Al_2O_3/TiO_2 has a wide peak range, which was concentrated at 20~50 nm and 60~90 nm, and the results showed that the layered mesoporous/macroporous structure was formed. Table 1 shows the distribution of specific surface area, pore volume, and pore size of the sample. The specific surface area and pore volume increased with the increase of Mn:Ce molar ratios from 1:2 to 4:1. However, the specific surface area and pore volume of Mn-Ce/Al_2O_3/TiO_2 decreased with further increasing of Mn:Ce molar ratios, because the agglomeration of the excess MnOx nanoparticles caused the blockage of some mesopores. It has been generally

acknowledged that the high specific surface areas were beneficial to promote the catalytic performance by offering more active sites.

Table 2. Catalyst pore structure data for different activity group distribution ratios.

Sample	S_{BET} (m^2/g)	V_p (cm^3/g)	D_p (nm)
Mn:Ce = 1:2	27.564	0.230	43.87
Mn:Ce = 2:1	30.131	0.269	45.25
Mn:Ce = 4:1	52.080	0.346	34.00
Mn:Ce = 5:1	26.134	0.229	41.61
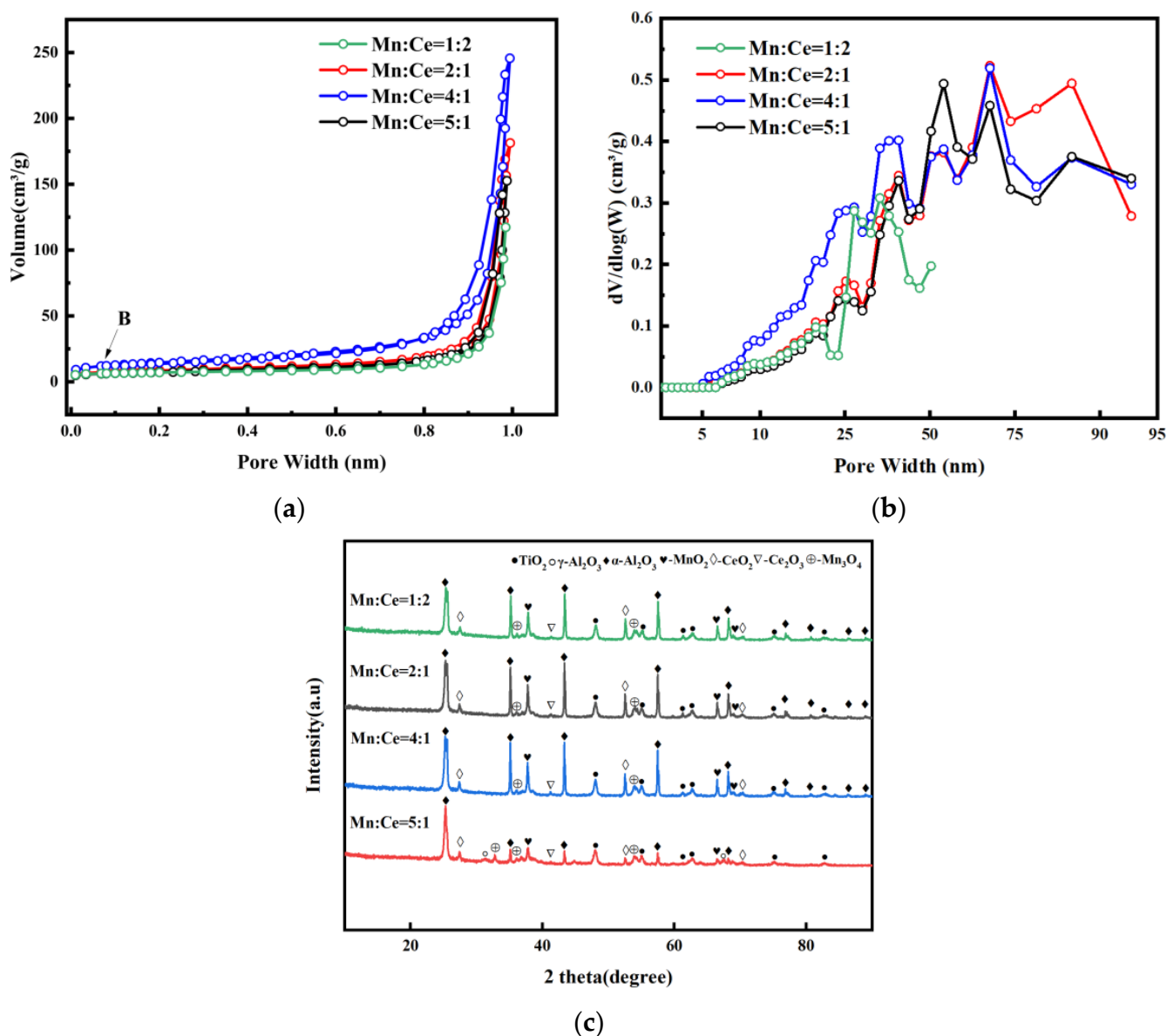
Figure 2. (**a**) N$_2$ adsorption and desorption isotherms of Mn-Ce/Al$_2$O$_3$/TiO$_2$ catalyst; (**b**) Pore size distribution curves of Mn-Ce/Al$_2$O$_3$/TiO$_2$ catalyst; (**c**) XRD patterns for Mn-Ce /Al$_2$O$_3$/TiO$_2$ catalyst.
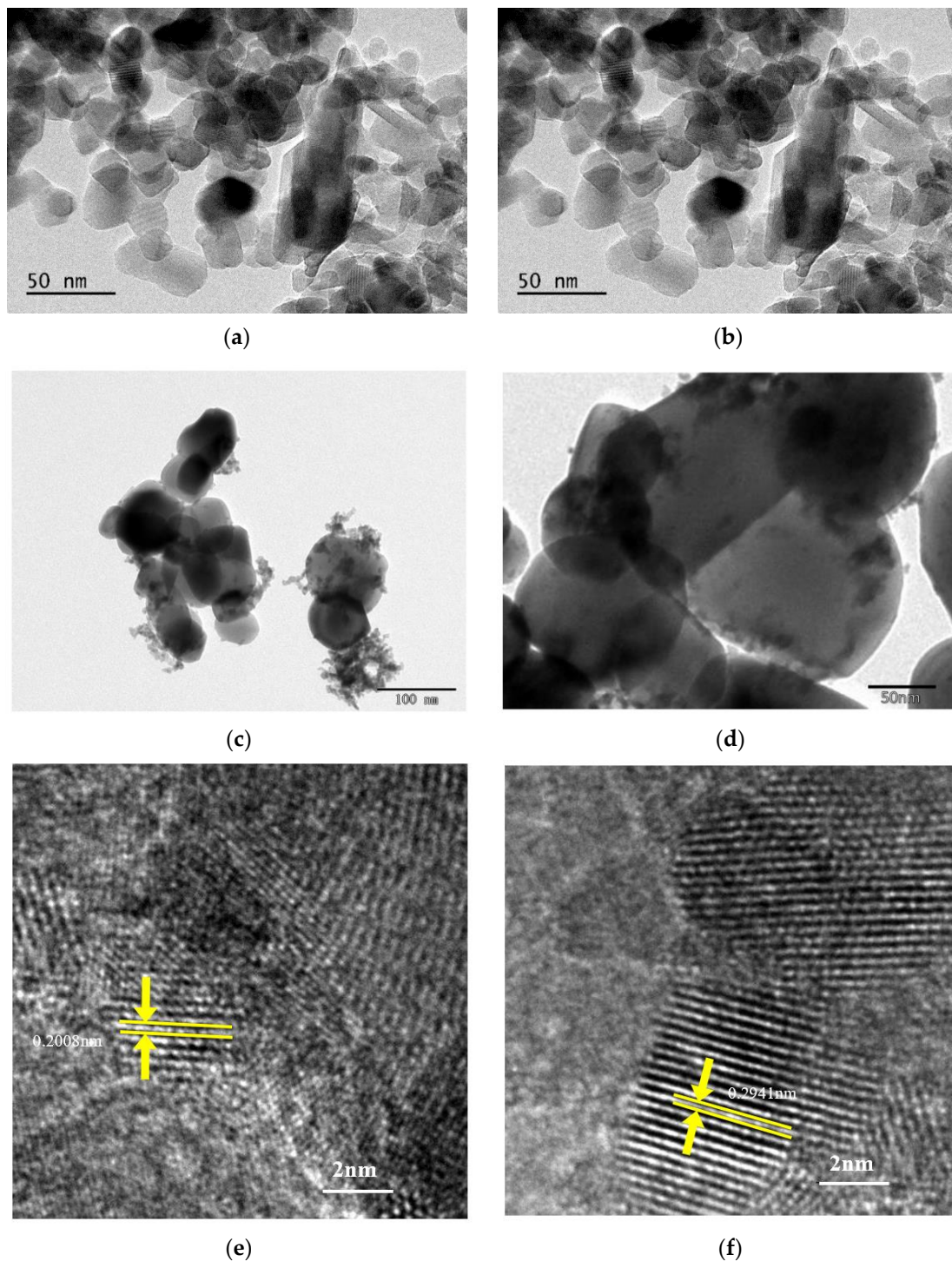
Figure 3. TEM images of Al_2O_3/TiO_2 (**a,b**); TEM images of Mn-Ce(4:1)/Al_2O_3/TiO_2 (**c,d**); HRTEM images of Mn-Ce(4:1)/Al_2O_3/TiO_2 (**e,f**).

XRD and TEM were used to analyze the structure of oxide and carrier components in the catalyst. Figure 2c shows the XRD patterns of catalysts prepared under the different molar ratios of Mn:Ce. XRD peaks at 2θ = 25.584, 37.784, 43.362, 57.581, 70.351, 76.880, 84.375, 86.375, 89.018 are attributed to α-Al_2O_3 (JCPDS 10-0173). XRD peaks at 2θ = 31.988, 66.761 are attributed to the γ-Al_2O_3 (JCPDFs 29-0063). There is no γ-Al_2O_3 peak in the XRD results of Mn:Ce = 1:2, Mn:Ce = 2:1, Mn:Ce = 4:1, the main reason may be that Mn ions promote the conversion of γ-alumina [18]. However, γ-Al_2O_3 was detected at Mn:Ce = 5:1 and γ-Al_2O_3 appeared at 2θ = 31.988, 66.761. The possible reason is that the interaction

between Mn-Ce is strengthened [19], and the effect of Mn ions is weakened, so γ-Al_2O_3 was preserved. XRD peaks at 2θ = 48.049, 53.890, 62.119, 62.688, 75.029, 82.659, are attributed to the anatase TiO_2 (JCPDS 21-1272). XRD peaks at 2θ = 31.015, 36.085, 53.859, corresponding to 200, 211, 312 of Mn_3O_4 (JCPDFs 24-0734). When Mn:Ce = 5:1, the peaks of Mn_3O_4 began to increase (a diffraction peak of Mn_3O_4 appeared at 32.441). With the increase of the amount of Mn ion recombination, the Mn_3O_4 phase increased, mainly due to the coexistence of MnO_2 and Mn_3O_4 phases [20]. XRD peaks at 2θ = 37.685, 66.815, 68.594, corresponding to 011, 310, 130 of MnO_2 (JCPDFs 50-0866) [21]. According to the calculation results of the Scherrer equation, it was found that the crystalline size was 17.8 nm at Mn:Ce = 1:2, 15.7 nm at Mn:Ce = 2:1, 16.3 nm at Mn:Ce = 4:1, and 13.8 nm at Mn:Ce = 5:1. It can be seen that in the case of Mn:Ce = 5:1, its crystalline size was the smallest. From the crystallinity and crystalline size of MnO_2, it can be seen that the crystallinity of MnO_2 decreased and the grain size decreased, indicating that the increase of Mn:Ce ratio inhibited the growth of MnO_2 crystalline [22]. At the same time, combined with the removal efficiency of NO under different Mn:Ce, it can be seen that the change of crystallinity of MnO_2 in the catalyst has a certain influence on the catalytic performance of the catalyst. In addition, XRD peaks at 2θ = 37.868, corresponding to 332 of Ce_2O_3 (JCPDFs 49-1458). XRD peaks at 2θ = 27.334, 52.649, and 70.478, corresponding to 112, 006, and 226 of CeO_2 (JCPDFs 44-1001). With the increase of Mn content, the peak intensity of CeO_2 changed slightly. It is most obvious at 52.649, possibly because the crystallinity of CeO_2 decreased due to the limitation of the crystallite growth of CeO_2 with the increase of the recombination amount of Mn ions [13].

It can be seen from the TEM of Figure 3a,b that the Al_2O_3/TiO_2 was a uniform size nanoblock. The Al_2O_3/TiO_2 nanoblocks ranged from 45–80 nm, and the average nanoblock size was about 60 nm, and it can be clearly seen that there was an obvious heterojunction between Al_2O_3 and TiO_2. It can be seen from Figure 3c,d that the active components of Mn-Ce were uniform nanospheres. The average diameter of the nanospheres was about 2 nm, and the active components of Mn-Ce were evenly distributed on the surface of the Al_2O_3/TiO_2 carrier. The Mn-Ce like particles and Al_2O_3/TiO_2 like blocks were observed, which indicated that the complex contained two morphologies: particle and bulk. Figure 3e,f shows the typical HRTEM image of Mn-Ce(4:1)/Al_2O_3/TiO_2. The observed spacing between the lattice planes of the sample was measured to be 0.2008 nm and 0.2941 nm, matched with (312) crystal plane of Mn_3O_4 and (310) crystal plane of MnO_2, respectively. Therefore, the morphology of Mn-Ce/Al_2O_3/TiO_2 prepared by impregnation method was uniform, the active components were evenly dispersed, and no agglomeration occurred, which indicated that the simple impregnation method can be used to prepare the nano-catalyst with uniform morphology. At the same time, combined with XRD analysis, it can be seen that there was a mutual reaction between the Mn-Ce active component and the carrier Al_2O_3/TiO_2, and there was an interfacial link between the components.

3.2. Catalyst Performance Analysis

Figure 4a shows the efficiency of catalysts with different Mn:Ce molar ratios for the catalytic ozonation of NO when the volume of O_3:NO = 1:4. As can be seen from Figure 4a, when the volume ratio of O_3:NO remained unchanged, the temperature had a certain influence on NO removal. With the increase of temperature, NO removal by different ratios of active component catalysts changed greatly. Overall, the Mn-Ce (4:1)/Al_2O_3/TiO_2 catalyst was more stable and efficient than other catalysts for NO removal. Different components had a great influence on NO removal, and when the molar ratio of Mn:Ce = 1:4, the catalyst had a good and stable performance [13]. Low-concentration ozone (the volume ratio of O_3:NO < 2, O_3 concentration < 150 ppm) was mainly used in this experiment. According to the experimental data, the sum of the volume concentrations of NO and NO_2 after the reaction was equivalent to the volume concentration of NO before the reaction. It can be seen that ozone mainly oxidized NO to NO_2, and there were no other types of N-containing oxides. The reaction of ozone oxidation of NO was shown in Equation (2) [11].
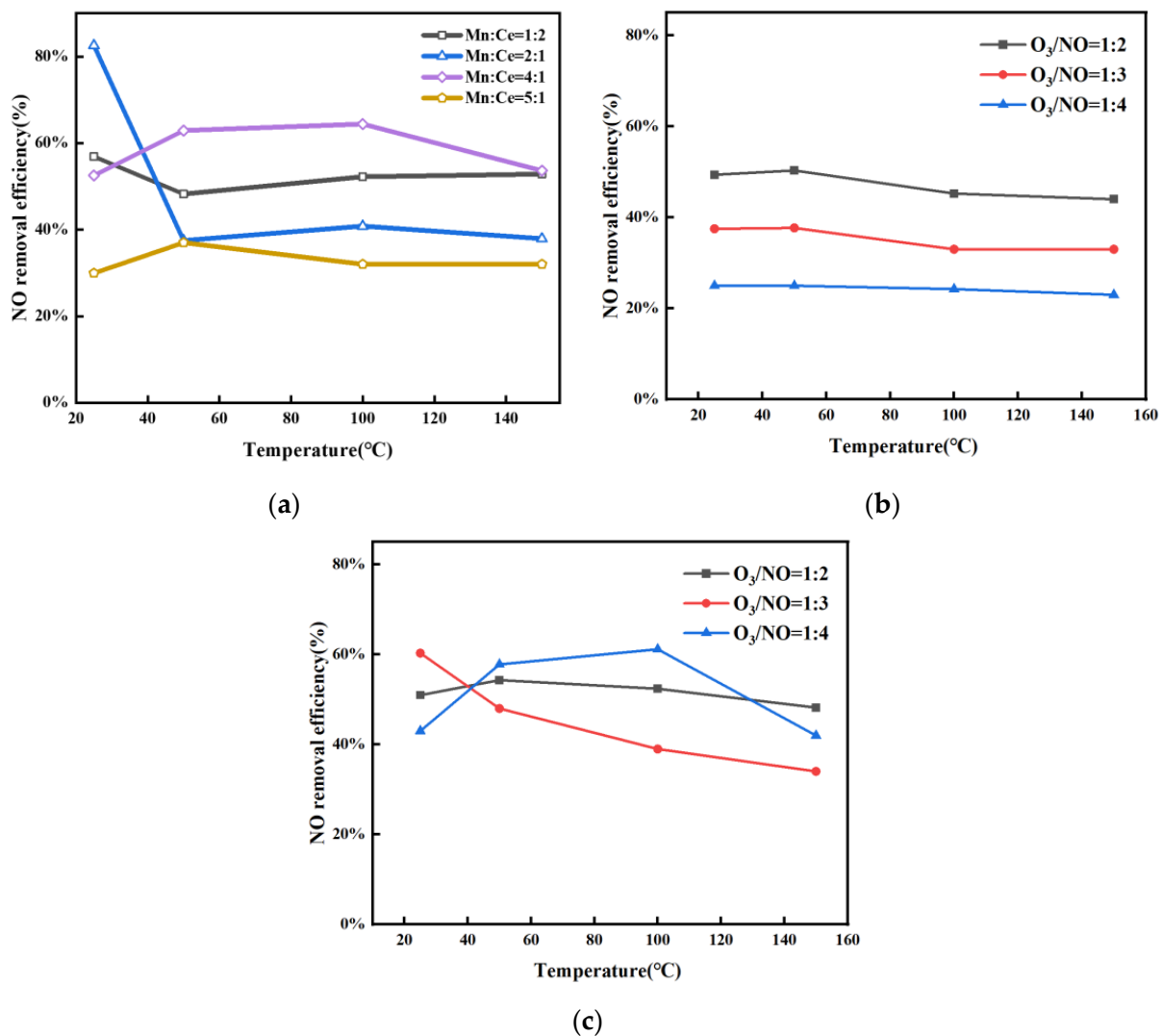
Figure 4. (**a**) The efficiency of catalysts with different Mn:Ce molar ratios for the catalytic ozonation of NO when the volume of O_3:NO = 1:4; (**b**) The effect of increasing the ratio of O_3 on NO removal without catalyst; (**c**) Under the synergistic catalysis of Mn-Ce (4:1)/Al_2O_3/TiO_2 catalyst, increasing the ratio of O_3 on NO removal Impact.

Figure 4b shows the effect of increasing the ratio of O_3 on NO removal without a catalyst. As can be seen from Figure 4b, when O_3:NO = 1:4, the average NO removal rate was 24%, when O_3:NO = 1:3, the average NO removal rate was 35%, and when O_3:NO = 1:2, the average removal rate of NO was 47%. With the increased O_3 ratio, the removal rate of NO increased gradually. Figure 4c shows the improvement of NO removal rate of O_3 under the co-catalysis of Mn-Ce (4:1)/Al_2O_3/TiO_2 catalyst. It can be found that under the catalysis of Mn-Ce (4:1)/Al_2O_3/TiO_2 catalyst, when O_3:NO = 1:4, the average NO removal rate was 51%, and when O_3:NO = 1:3, the average NO removal rate was 45%. When O_3:NO = 1:2, the average NO removal efficiency was 51%. Compared with Figure 4b,c, it can be seen that under the action of the catalyst, with the increase of O_3 concentration, the NO removal rate decreased. This is due to the fact that under the conditions of higher concentration of ozone, the initial NO_2 concentration was relatively high, and then the catalyst is easier to catalyze ozone to promote the conversion of NO_2 to N_2O_5, which reduced the reaction between O_3 and NO, and reduced the removal rate of NO [15]. Therefore, the conversion of NO to NO_2 was more readily promoted at lower ozone concentrations in the presence of catalysts. This study provided an opportunity to improve NO removal using catalyst catalysis at lower ozone concentrations, both to improve ozone utilization and to reduce ozone leakage.

The removal of NOx by ozone oxidation + alkali absorption in the presence of catalyst is shown in Figure 5. When the initial NO concentration was 200 ppm, the volume ratio of O_3:NO was 1:4, the molar ratio of Mn:Ce was 4:1, the concentration of NaOH was 5 wt%, the NO outlet concentration was 36 ppm, the NO_2 emission concentration was 7 ppm, and the overall NOx emission concentration was 43 ppm, which could meet the relevant flue gas emission requirements. The main reaction equations for NO and NO_2 in NaOH solution are shown in Equations (7) and (8). As time goes on, the removal efficiency of NO_2 gradually decreased, but remained above 85% overall, while the removal efficiency of NO increased gradually with time. Higher concentrations of NO_2 mainly occurs in Equation (8). With the progress of the reaction, the pH of the absorption solution gradually decreased, and Equation (7) gradually became the main reaction. So the removal rate of NO gradually increased and the amount of NO_2 removed decreased [11].

$$NO + NO_2 + 2NaOH \rightarrow 2NaNO_2 + H_2O, \tag{7}$$

$$2NO_2 + 2NaOH \rightarrow NaNO_2 + NaNO_3 + H_2O, \tag{8}$$
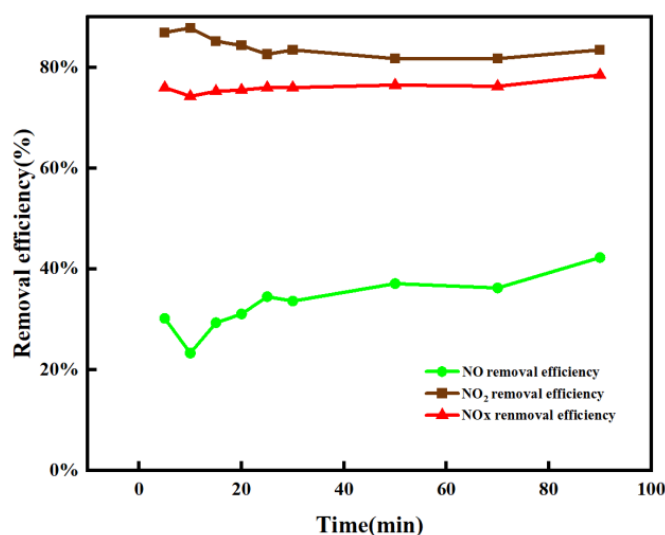
Figure 5. Removal of NOx by NaOH solution (O_3:NO = 1:4, Mn:Ce = 4:1, 5 wt% NaOH).

The distribution of Mn, Ce, and O elements on the surface of the catalyst was analyzed by XPS. Figure 6a is the XPS spectrum of Mn 2p. The Mn 2p XPS spectra showed two characteristic peaks of Mn 2p1/2 and Mn 2p3/2. The Mn 2p3/2 peak at 640.3 ev, 642.8 ev, 643.4 ev are attributed to Mn^{2+}, Mn^{3+}, and Mn^{4+} species [23]. The Mn 2p1/2 peak at 652.2 ev, 653.1 ev, 653.9 ev are attributed to Mn Mn^{2+}, Mn^{3+}, and Mn^{4+} species [24]. Figure 6a,b showed the XPS spectra of the catalyst (Mn:Ce = 1:2). Mn^{4+} was detected only at 638.3 eV, so the Mn ion content of Mn:Ce = 4:1 catalyst was more, and mainly increased Mn^{3+}. Related studies have shown that Mn^{4+} can promote the generation of reactive oxygen species (O*) from ozone, and the presence of Mn^{3+} lead to the generation of oxygen vacancies and promoted the generation of O* from ozone, both of which can enhance the performance of NO oxidation by ozone [25]. Therefore, Mn:Ce = 4:1 catalyst is more efficient than Mn:Ce = 1:2 catalyst in promoting ozonation of NO. Table 3 shows the proportion of Mn ions, Ce ions, and O species in the catalyst calculated based on XPS results. According to its distribution, it can be seen that under Mn:Ce = 4:1, the content of Mn^{2+} is the largest. Under ozone conditions, high proportion of Mn^{2+} promoted the conversion to Mn^{3+} and Mn^{4+}. Figure 6b is the XPS spectrum of Ce 3d showed two characteristic peaks of Ce 3d5/2 and Ce3d3/2. It can be seen that under Mn:Ce = 1:2, the peaks V″ (887.8 ev), U (881.3 ev), V′ (903.7 ev), V″ (907.1 ev), V″″ (908.3 ev) are attributed to Ce^{3+}; the peaks U^0 (882.3 ev), U′ (886.3 ev), U‴ (888.4 ev), U″″ (888.6 ev), U′V″″ (898.3 ev), V (900.8 ev), V^0 (900.9 ev),

V′′′ (907.3 ev), V′V′′′′ (916.7 ev) are attributed to Ce^{4+}. It can be seen that under Mn:Ce = 4:1, the peaks 880.7 ev, 884.0 ev, 885.5 ev, 886.0 ev, 900.7 ev, 903.9 ev, 907.1 ev are attributed to Ce^{3+}; the peaks 881.1 ev, 900.8 ev, 900.9 ev, 916.0 ev, 916.7 ev are attributed to Ce^{4+}. According to Table 3, when Mn:Ce = 4:1, Ce^{3+} accounted for a large proportion, and a large amount of Ce^{3+} helped to generate O^{2-}, and O^{2-} helped to promote the mutual conversion between Mn ions, which in turn promoted the decomposition of ozone into O* [26], which indirectly indicated that the Mn:Ce = 4:1 catalyst has higher catalytic activity. In Figure 6c, the XPS patterns of O 1 s showed the presence of two types of surface oxygen in the Mn-Ce/Al$_2$O$_3$/TiO$_2$ catalysts. The fitted peaks could be attributed to lattice oxygen O (lat) (529.5 eV) and chemisorbed oxygen (abs) (532.17 ev, 532.5 ev). It was well recognized that O (abs) species were more active in promoting ozone generation of O* than O (lat) due to their higher mobility [27–29]. Figure 6c and Table 3 show that the surface concentration of O (abs) species over Mn-Ce (4:1)/Al$_2$O$_3$/TiO$_2$ was higher than Mn-Ce (1:2)/Al$_2$O$_3$/TiO$_2$, which was another reason for its higher catalytic activity compared with Mn-Ce (1:2)/Al$_2$O$_3$/TiO$_2$.
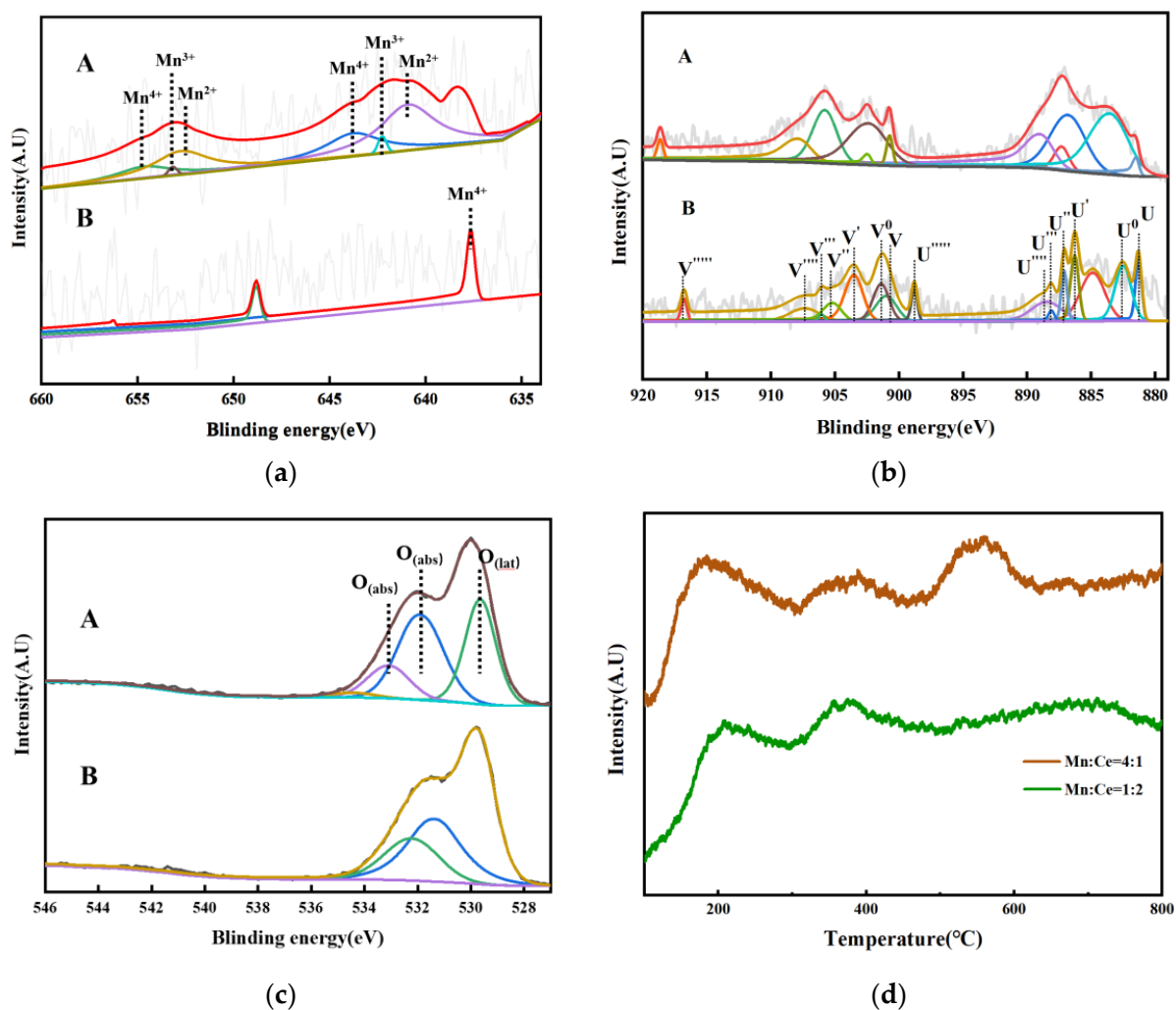
Figure 6. (**a**) XPS spectra of Mn 2p: A. Mn:Ce = 4:1; B. Mn:Ce = 1:2; (**b**) XPS spectra of Ce 3d: A. Mn:Ce = 4:1; B. Mn:Ce = 1:2; (**c**) XPS spectra of O 1 s: A. Mn:Ce = 4:1; B. Mn:Ce = 1:2; (**d**) O$_2$-TPD profile of Mn-Ce/Al$_2$O$_3$/TiO$_2$ catalysts (Mn:Ce = 4:1, Mn:Ce = 1:2).

Table 3. Distribution of Mn ions, Ce ions, and O species of synthesis catalysts based on XPS results.

Samples	$Mn^{2+}/(Mn^{2+} + Mn^{3+} + Mn^{4+})$ (%)	$Mn^{3+}/(Mn^{2+} + Mn^{3+} + Mn^{4+})$ (%)	$Mn^{4+}/(Mn^{2+} + Mn^{3+} + Mn^{4+})$ (%)	Ce^{3+}/Ce^{4+}	O (lat)	O (lat)/O (abs)
Mn:Ce = 4:1	40.18	26.61	33.21	1.29	38.03	0.51
Mn:Ce = 1:2	/	/	/	0.57	37.65	0.95

O_2-TPD results can be used to represent the type of oxygen species on the catalyst. O (abs) is more easily desorbed than O (lat) and will desorb at lower temperatures. O (abs) generally contains both physically adsorbed oxygen and chemisorbed oxygen, of which physically adsorbed oxygen is usually more easily desorbed than chemisorbed oxygen [30]. As depicted in Figure 6d, two peaks appeared at around 200 °C and 400 °C, which are the characteristic peaks of O (abs); the peak at 600 °C is mainly O (lat). When Mn:Ce = 4:1, more peaks appear when the temperature rises, indicating that there are more oxygen species on the catalyst surface. The desorption capacity of surface oxygen species contributes to improving the oxidation capacity of catalysts.

3.3. Reaction Mechanism

The process mechanism of catalysts promoting O_3 oxidation of NO can be summarized as follows: The catalyst contains large amounts of Mn (II), Mn (III), and Mn (IV). In the ozone atmosphere, Mn (II) and Mn (III) were oxidized and O* was produced at the same time. In combination with Section 3.2, catalyst and ozone have an excellent effect on NO removal, and the effect of O* can be inferred as Equations (9)–(11). NO was combined with O* to form NO•O* in the adsorption state. The adsorbed (NO•O*) will form (NO•O*)$_2$ and react with O_2 in the gas phase to form NO_2. The O^{2-} produced by the oxidation reaction between Ce (III) and Ce (IV) in the catalyst contributes to the transformation of Mn (IV) to Mn (II). It can be concluded that the oxidation reaction process of Mn (II) and Mn (III) in the ozone atmosphere is the main reaction promoting the oxidation of NO to NO_2. The oxidation-reduction reaction in Ce (III) and Ce (IV) and the oxygen species on the catalyst can promote the oxidation reaction of Mn (II) and Mn (III) in the ozone atmosphere. The reaction pathway is shown in Figure 7. The main reactions here are as follows:

$$NO + O* \rightarrow NO \cdot O*, \tag{9}$$

$$NO \cdot O* + NO \cdot O* \rightarrow (NO \cdot O*)_2, \tag{10}$$

$$(NO \cdot O*)_2 + O_2 \rightarrow 2NO_2 + 2O*, \tag{11}$$

$$Mn^{3+} + O_3 \rightarrow Mn^{4+} + O* + O_2, \tag{12}$$

$$Mn^{2+} + O_3 \rightarrow Mn^{3+} + O* + O_2, \tag{13}$$

$$Mn^{2+} + O_3 \rightarrow Mn^{4+} + O^{2-} + O_2, \tag{14}$$

$$Mn^{4+} + O^{2-} + O_3 \rightarrow Mn^{2+} + O_2, \tag{15}$$

$$Ce^{4+} + Mn^{3+} + O^{2-} \rightarrow Ce^{3+} + Mn^{4+}, \tag{16}$$

$$Ce^{3+} + O_2 \rightarrow Ce^{4+} + O^{2-}, \tag{17}$$
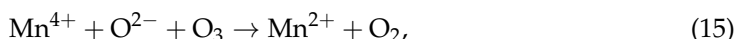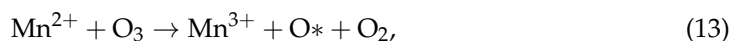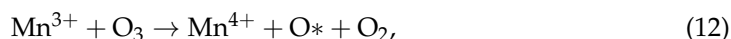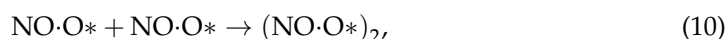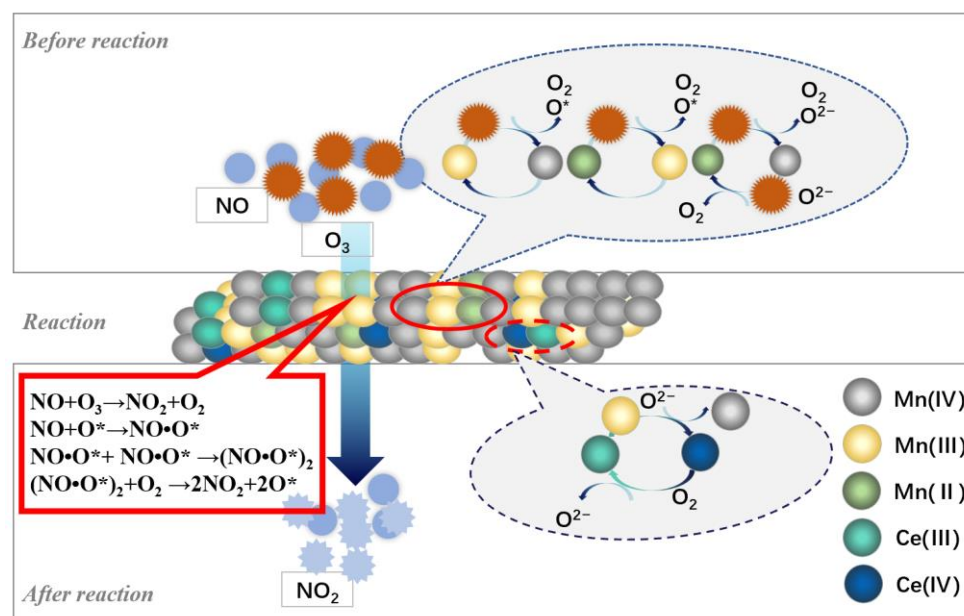
Figure 7. Reaction pathway of Mn-Ce/Al$_2$O$_3$/TiO$_2$ synergistic ozone oxidation of NO.

4. Conclusions

The experimental results show that the catalyst can significantly improve the efficiency of ozone oxidation of NO and reduce the amount of ozone. Based on the experimental results, the main conclusions are as follows:

1. The Mn-Ce/Al$_2$O$_3$/TiO$_2$ catalyst was prepared by the impregnation method. The catalysts were characterized by BET, XRD, TEM, XPS, and O$_2$-TPD. The results show that the catalysts have a large specific surface area (52.080 m^2/g) and pore volume (0.346 cm^3/g). High-specific surface areas are beneficial to promote the catalytic performance by offering more active sites. The catalyst mainly contains particle and bulk morphology, and the active components (MnOx, CeOx) are uniformly dispersed, and no agglomeration occurs. At the same time, the catalyst contains a large number of CeOx, O (lat), and O (abs) species. The content of MnOx, oxygen species on the surface of the catalyst, is the factor affecting the activity of the catalyst.

2. The mechanism study shows that the MnOx content on the catalyst surface is the main factor affecting the catalyst activity. The presence of Mn^{2+} and Mn^{3+} on the surface of the catalyst can promote the decomposition of ozone to produce O*. O^{2-} contributes to the reduction reaction between Mn^{2+} and Mn^{4+}, and O* and oxygen species on the catalyst surface significantly promote the oxidation of NO to NO$_2$.

3. Under the experimental conditions of flue gas temperature 100–150 °C, the molar ratio of Mn:Ce = 4:1, the volume ratio of O$_3$:NO = 1:4, and the NO removal rate can reach 63%. Compared with the oxidation of NO by ozone alone, the oxidation efficiency of NO can be increased by 40% by adding a catalyst. The experimental results show that the prepared catalyst can significantly improve the efficiency of ozone oxidation of NO and reduce the amount of ozone. After NaOH absorption, the NOx removal efficiency achieves up to 79.6% for the O$_3$ + Mn-Ce (4:1)/Al$_2$O$_3$/TiO$_2$ method, which can well meet the NOx emission standard in China.

Author Contributions: Writing—original draft preparation, H.S.; writing—review and editing, H.S., Z.T., X.X., H.W., H.Z., P.F., D.Z. and J.G. All authors have read and agreed to the published version of the manuscript.

Funding: This work was supported by the Special Funds for Basic Research Operations of Public Welfare Research Institutes (PM-zx703-202204-142), the Support Program for Outstanding Young Scientific and Technological Talents, South China Institute of Environmental Sciences (PM-zx421-202104-104), and Ministry of Ecology and Environment, Science and Technology Plan Project of Guangdong Province (2018B020208002).

Institutional Review Board Statement: Not applicable.

Informed Consent Statement: Not applicable.

Data Availability Statement: Not applicable.

Acknowledgments: Authors gratefully acknowledge the South China Institute of Environmental Science of the Ministry of Ecology and Environment for their support for this research.

Conflicts of Interest: The authors declare no conflict of interest.

References

1. Lin, F.; Wang, Z.; Zhang, Z.; He, Y.; Zhu, Y.; Shao, J.; Yuan, D.; Chen, G.; Cen, K. Flue Gas Treatment with Ozone Oxidation: An Overview on NOx, Organic Pollutants, and Mercury. *Chem. Eng. J.* **2020**, *382*, 123030. [CrossRef]
2. Ren, X.; Sun, R.; Meng, X.; Vorobiev, N.; Schiemann, M.; Levendis, Y.A. Carbon, Sulfur and Nitrogen Oxide Emissions from Combustion of Pulverized Raw and Torrefied Biomass. *Fuel* **2017**, *188*, 310–323. [CrossRef]
3. Andreae, M.O. Emission of Trace Gases and Aerosols from Biomass Burning—An Updated Assessment. *Atmospheric Chem. Phys.* **2019**, *19*, 8523–8546. [CrossRef]
4. Bhutto, A.W.; Bazmi, A.A.; Karim, S.; Abro, R.; Mazari, S.A.; Nizamuddin, S. Promoting Sustainability of Use of Biomass as Energy Resource: Pakistan's Perspective. *Environ. Sci. Pollut. Res.* **2019**, *26*, 29606–29619. [CrossRef]
5. Zhai, J.; Burke, I.T.; Stewart, D.I. Beneficial Management of Biomass Combustion Ashes. *Renew. Sustain. Energy Rev.* **2021**, *151*, 111555. [CrossRef]
6. Suzuki, K.; Tsuji, N.; Shirai, Y.; Hassan, M.A.; Osaki, M. Evaluation of Biomass Energy Potential towards Achieving Sustainability in Biomass Energy Utilization in Sabah, Malaysia. *Biomass Bioenergy* **2017**, *97*, 149–154. [CrossRef]
7. Brosowski, A.; Krause, T.; Mantau, U.; Mahro, B.; Noke, A.; Richter, F.; Raussen, T.; Bischof, R.; Hering, T.; Blanke, C.; et al. How to Measure the Impact of Biogenic Residues, Wastes and by-Products: Development of a National Resource Monitoring Based on the Example of Germany. *Biomass Bioenergy* **2019**, *127*, 105275. [CrossRef]
8. Abid, S.; Zhang, X.; Zhang, W.; Mu, H.; Zhang, C.; Wang, A. System Performance and Pollution Emission of Biomass Gas Co-Firing in a Coal-Fired Boiler. *J. Power Energy Eng.* **2020**, *8*, 18–25. [CrossRef]
9. Hillig, D.M.; Pohlmann, J.G.; Manera, C.; Perondi, D.; Pereira, F.M.; Altafini, C.R.; Godinho, M. Evaluation of the Structural Changes of a Char Produced by Slow Pyrolysis of Biomass and of a High-Ash Coal during Its Combustion and Their Role in the Reactivity and Flue Gas Emissions. *Energy* **2020**, *202*, 117793. [CrossRef]
10. Cai, S.; Zhang, D.; Zhang, L.; Huang, L.; Li, H.; Gao, R.; Shi, L.; Zhang, J. Comparative Study of 3D Ordered Macroporous $Ce_{0.75}Zr_{0.2}M_{0.05}O_2-\delta$ (M = Fe, Cu, Mn, Co) for Selective Catalytic Reduction of NO with NH_3. *Catal. Sci. Technol.* **2013**, *4*, 93–101. [CrossRef]
11. Zhang, J.; Zhang, R.; Chen, X.; Tong, M.; Kang, W.; Guo, S.; Zhou, Y.; Lu, J. Simultaneous Removal of NO and SO_2 from Flue Gas by Ozone Oxidation and NaOH Absorption. *Ind. Eng. Chem. Res.* **2014**, *53*, 6450–6456. [CrossRef]
12. Zhang, Z.; Xiang, L.; Lin, F.; Wang, Z.; Yan, B.; Chen, G. Catalytic Deep Degradation of Cl-VOCs with the Assistance of Ozone at Low Temperature over MnO_2 Catalysts. *Chem. Eng. J.* **2021**, *426*, 130814. [CrossRef]
13. Rezaei, E.; Soltan, J.; Chen, N. Catalytic Oxidation of Toluene by Ozone over Alumina Supported Manganese Oxides: Effect of Catalyst Loading. *Appl. Catal. B Environ.* **2013**, *136–137*, 239–247. [CrossRef]
14. Jõgi, I.; Erme, K.; Raud, J.; Laan, M. Oxidation of NO by Ozone in the Presence of TiO_2 Catalyst. *Fuel* **2016**, *173*, 45–51. [CrossRef]
15. Lin, F.; Wang, Z.; Ma, Q.; Yang, Y.; Whiddon, R.; Zhu, Y.; Cen, K. Catalytic Deep Oxidation of NO by Ozone over MnOx Loaded Spherical Alumina Catalyst. *Appl. Catal. B Environ.* **2016**, *198*, 100–111. [CrossRef]
16. Meng, F.; Guo, L.; He, J.; Wang, Z.; Ma, Z.; Zeng, Y.; Zhang, S.; Zhong, Q. V_2O_5-$(NH_4)_2V_6O_{16}\cdot1.5H_2O$ Composite Catalysts as Novel Platforms for High-Efficiency Catalytic Ozonation of NO under Low Temperature. *J. Phys. Chem. Solids* **2021**, *155*, 110112. [CrossRef]
17. Guo, L.; Meng, F.; Zeng, Y.; Jia, Y.; Qian, F.; Zhang, S.; Zhong, Q. Catalytic Ozonation of NOx into HNO_3 with Low Concentration Ozone over MnOx-CeO_2/TiO_2: Two-Phase Synergistic Effect of TiO_2. *Mol. Catal.* **2020**, *493*, 111095. [CrossRef]
18. Okada, K.; Hattori, A.; Taniguchi, T.; Nukui, A.; Das, R.N. Effect of Divalent Cation Additives on the γ-Al_2O_3-to-α-Al_2O_3 Phase Transition. *J. Am. Ceram. Soc.* **2004**, *83*, 928–932. [CrossRef]
19. Shao, S.; Li, Z.; Zhang, J.; Gao, K.; Liu, Y.; Jiao, W. Preparation of Ce-MnOX/γ-Al_2O_3 by High Gravity-Assisted Impregnation Method for Efficient Catalytic Ozonation. *Chem. Eng. Sci.* **2022**, *248*, 117246. [CrossRef]
20. Yao, X.; Li, L.; Zou, W.; Yu, S.; An, J.; Li, H.; Yang, F.; Dong, L. Preparation, Characterization, and Catalytic Performance of High Efficient CeO_2-MnOx-Al_2O_3 Catalysts for NO Elimination. *Chin. J. Catal.* **2016**, *37*, 1369–1380. [CrossRef]

21. Zhang, X.; Liu, Y.; Deng, J.; Yu, X.; Han, Z.; Zhang, K.; Dai, H. Alloying of Gold with Palladium: An Effective Strategy to Improve Catalytic Stability and Chlorine-Tolerance of the 3DOM CeO$_2$-Supported Catalysts in Trichloroethylene Combustion. *Appl. Catal. B Environ.* **2019**, *257*, 117879. [CrossRef]

22. Lin, X.; Li, S.; He, H.; Wu, Z.; Wu, J.; Chen, L.; Ye, D.; Fu, M. Evolution of Oxygen Vacancies in MnOx-CeO$_2$ Mixed Oxides for Soot Oxidation. *Appl. Catal. B Environ.* **2018**, *223*, 91–102. [CrossRef]

23. Mu, W.; Zhu, J.; Zhang, S.; Guo, Y.; Su, L.; Li, X.; Li, Z. Novel Proposition on Mechanism Aspects over Fe-Mn/ZSM-5 Catalyst for NH$_3$-SCR of NO:X at Low Temperature: Rate and Direction of Multifunctional Electron-Transfer-Bridge and in Situ DRIFTs Analysis. *Catal. Sci. Technol.* **2016**, *6*, 7532–7548. [CrossRef]

24. Li, Q.; Li, X.; Li, W.; Zhong, L.; Zhang, C.; Fang, Q.; Chen, G. Effect of Preferential Exposure of Anatase TiO$_2$ {001} Facets on the Performance of Mn-Ce/TiO$_2$ Catalysts for Low-Temperature Selective Catalytic Reduction of NOx with NH$_3$. *Chem. Eng. J.* **2019**, *369*, 26–34. [CrossRef]

25. Lin, F.; Wang, Z.; Zhang, Z.; Xiang, L.; Yuan, D.; Yan, B.; Wang, Z.; Chen, G. Comparative Investigation on Chlorobenzene Oxidation by Oxygen and Ozone over a MnOx/Al$_2$O$_3$ Catalyst in the Presence of SO$_2$. *Environ. Sci. Technol.* **2021**, *55*, 3341–3351. [CrossRef] [PubMed]

26. Gonçalves, A.; Silvestre-Albero, J.; Ramos-Fernandez, E.V.; Ruiz, J.C.S.; Órfão, J.; Sepúlveda-Escribano, A.; Pereira, M.F. Highly Dispersed Ceria on Activated Carbon for the Catalyzed Ozonation of Organic Pollutants. *Appl. Catal. B Environ.* **2012**, *113–114*, 308–317. [CrossRef]

27. Ye, B.; Kim, J.; Lee, M.; Chun, S.-Y.; Jeong, B.; Kim, T.; Lee, D.H.; Kim, H.-D. Mn-Ce Oxide Nanoparticles Supported on Nitrogen-Doped Reduced Graphene Oxide as Low-Temperature Catalysts for Selective Catalytic Reduction of Nitrogen Oxides. *Microporous Mesoporous Mater.* **2021**, *310*, 110588. [CrossRef]

28. Wang, Y.; Deng, W.; Wang, Y.; Guo, L.; Ishihara, T. A Comparative Study of the Catalytic Oxidation of Chlorobenzene and Toluene over Ce-Mn Oxides. *Mol. Catal.* **2018**, *459*, 61–70. [CrossRef]

29. Zhang, X.; Zhao, J.; Song, Z.; Liu, W.; Zhao, H.; Zhao, M.; Xing, Y.; Ma, Z.; Du, H. The Catalytic Oxidation Performance of Toluene over the Ce-Mn-Ox Catalysts: Effect of Synthetic Routes. *J. Colloid Interface Sci.* **2020**, *562*, 170–181. [CrossRef]

30. Li, P.; He, C.; Cheng, J.; Ma, C.Y.; Dou, B.J.; Hao, Z.P. Catalytic Oxidation of Toluene over Pd/Co$_3$AlO Catalysts Derived from Hydrotalcite-like Compounds: Effects of Preparation Methods. *Appl. Catal. B Environ.* **2011**, *101*, 570–579. [CrossRef]